

## Fluidogenic Landforms within the Area of Permafrost Occurrence on the Shelf of the Pechora and Kara Seas

A. V. Kokhan<sup>a,\*</sup>, E. A. Moroz<sup>a,\*\*</sup>, E. A. Eremenko<sup>a,b,\*\*\*</sup>, A. P. Denisova<sup>a,b,\*\*\*\*</sup>,  
R. A. Ananiev<sup>c,\*\*\*\*\*</sup>, E. A. Sukhikh<sup>d,\*\*\*\*\*</sup>, S. L. Nikiforov<sup>c,\*\*\*\*\*</sup>,  
S. Yu. Sokolov<sup>a,\*\*\*\*\*</sup>, and A. A. Razumovskiy<sup>e,\*\*\*\*\*</sup>

<sup>a</sup> Laboratory of Geology and Tectonics of the Ocean Bottom, Geological Institute, Russian Academy of Sciences, Moscow, 119017 Russia

<sup>b</sup> Geographical Faculty, Department of Geomorphology and Palaeogeography, Moscow State University, Moscow, 119991 Russia

<sup>c</sup> Laboratory of Seismic Stratigraphy, Institute of Oceanology, Russian Academy of Sciences, Moscow, 117997 Russia

<sup>d</sup> Laboratory of Heat and Mass Transfer, Geological Institute, Russian Academy of Sciences, Moscow, 119017 Russia

<sup>e</sup> Laboratory of Geology of Folded Belts, Geological Institute, Russian Academy of Sciences, Moscow, 119017 Russia

\*e-mail: kkkkk1987@mail.ru

\*\*e-mail: morozzea@gmail.com

\*\*\*e-mail: eremenkoeaig@gmail.com

\*\*\*\*e-mail: anden6900@gmail.com

\*\*\*\*\*e-mail: corer@mail.ru

\*\*\*\*\*e-mail: sukhikh\_ea@mail.ru

\*\*\*\*\*e-mail: nikiforov@ocean.ru

\*\*\*\*\*e-mail: sysokolov@yandex.ru

\*\*\*\*\*e-mail: anatoly.razumovskiy@mail.ru

Received September 28, 2022; revised November 16, 2022; accepted December 1, 2022

**Abstract**—This research is based on the results of multibeam echo-sounding and high-frequency seismic profiling, carried out during the cruises of the R/V *Akademik Nikolai Strakhov* and *Akademik Boris Petrov* in 2018–2022. Regularities of changes of morphometric parameters and the internal structure of pingo-like features of the shelves of the Pechora and Kara seas were established. A morphometric analysis of pingo-like features was carried out, which made it possible to draw conclusions about their relative ages, as well as the degree of participation of the activity of near-bottom currents and slope processes in their modern dynamics. It was revealed that the density and morphological variety of pingo-like features depend on the geological and tectonic position of the bottom area, the presence and nature of permafrost, the intensity of degassing, and the timing of shelf flooding during the Holocene transgression. In areas of the shelf, where the depth exceeds 70–80 m, pingo-like features were formed at the early stages of the Holocene transgression; by now, the permafrost there has largely thawed. At the same time, pingo-like features retain their prominence in the relief and are actively transformed by the activity of bottom currents, slope and, possibly, pseudovolcanic processes associated with ongoing degassing. In shallow (up to 20–30 m) shelf areas close to the shore, pingo-like features are rare and, apparently, continue to form at the present time. At the same time, the large thickness and continuity of permafrost prevent active fluid flow, playing the role of a seal. Pingo-like features in the shallow-water are characterized by the morphology of cone-shaped mounds and the absence of signs of intensive degassing. At intermediate depths (from 20–30 to 70–80 m), in the presence of insular or discontinuous permafrost, under conditions of high fluid flow intensity in the area of fault zones and oil- and gas-bearing structures, the density of pingo-like features is maximal. In such areas, the localized processes of heaving and active degassing are combined in the near-surface sediments, this determines a wide variety of morphological types of pingo-like features.

**Keywords:** Arctic, bottom topography, degassing, pingo-like features, acoustic anomalies, multibeam echo sounding, seismoacoustic profiling

DOI: 10.3103/S0145875225700061

### INTRODUCTION AND PROBLEM STATEMENT

The shelf zone of the Arctic Ocean is its most studied part, but even here there are still many “blank

spots” that require detailed research. One of them is the phenomenon of degassing and the relief it creates. Degassing is the process of fluids, mainly methane, rising from the Earth’s interior up the section to the

bottom surface and into the water column (Judd and Hovland, 2007), leading to gas saturation of the sedimentary cover, the formation of fluidogenic relief (proposed for identification as a special genetic type of subaqueous bottom relief in (Mironyuk, 2020)), and the appearance of sediments in the water. The fluidogenic relief on the Arctic shelves of Russia is presented by pockmarks, pingo-like features, and pseudovolcanic formations, the description of which has been the subject of many scientific papers (Shearer et al., 1971; Paull et al., 2007; Serov et al., 2015; Mironyuk et al., 2019; Mironyuk, 2020). At the same time, issues related to the causes of degassing and sources of fluids, as well as the nature of the relationship between the geological and tectonic structure, geocryological conditions, and the intensity of degassing and the morphology of the fluidogenic relief, remain controversial. The object of study in this paper was pingo-like features (PLFs), which are presented on the shelves of the Pechora and Kara seas; the goal was a detailed characterization of the morphological parameters of PLFs, an assessment of their modern dynamics, and the identification of the relationship between the listed properties, conditions, and factors of bottom relief development.

Compared to other fluidogenic features, PLFs remain poorly studied. According to existing concepts (Bondarev et al., 2002; Portnov et al., 2013; Serov et al., 2015; Mironyuk et al., 2019; Paull et al., 2022), the formation of PLFs is caused by the release of gases associated with the melting of subaqueous permafrost and intra- and subpermafrost gas hydrates, as well as the rise of deep thermogenic gases to the surface. PLFs were first discovered on the continental shelf of the Beaufort Sea in 1969 (Shearer et al., 1971). Based on morphological features, they were interpreted as relict (subaerial) cryogenic frost mounds. Further studies have shown that they are confined to the edge of the shelf and fault zones in its interior, where permafrosts have an insular distribution and pinch out (Paull et al., 2007, 2022). It has been established that PLFs are composed of sandy loam and sandy soils, thawed low-plasticity loams, loams with high ice content and ice-rich soils with ice contents from 10–30 to 70–90% (Paull et al., 2007). In the axial part of the PLF, gas flares were often observed; the molecular composition and carbon isotope of the methane in the gas emissions indicated that the gas originated from subpermafrost and intrapermafrost gas hydrate deposits (Paull et al., 2007). It was suggested that the melting of gas hydrates led to the formation of zones of abnormally high reservoir pressure and the involvement of plastic frozen sediments with high ice content in the movement upward through the section along weakened zones and areas of reduced permafrost thickness (Paull et al., 2007). Subsequent bottom rock sampling and surveys using underwater autonomous and remotely operated vehicles showed that PLFs are formed at depths of 100–130 m, whose genesis is pos-

sibly associated with the influx of groundwater from land (from the Mackenzie River basin) along the base of the permafrost to the shelf edge, thawing and melting of permafrost (Paul et al., 2021).

In the waters of Russian Arctic seas, PLFs were first discovered and surveyed during the work of the Arctic Marine Engineering-Geological Expeditions (AMEGE) State Unitary Enterprise in 1988 in the northeastern part of the Pechora Sea (Bondarev et al., 2002). In 1995–1996, drilling, seismic profiling and hydrolocation were carried out here over an area of  $5 \times 5$  km. Continuous seismic profiling data showed that the PLFs are composed of sediments of an acoustically opaque seismic complex, while within the compensatory depressions separating them the acoustic signal was completely absorbed. PLFs drilling showed that the acoustically opaque seismic complex is represented by Kazantsevo loams and clays with high ice contents decreasing from 90% in the near-surface to 30% in the lower part of the section. In the apical part of one of the pingo-like features, an abnormally pressured zone was uncovered in the Zyryan sands underlying the Kargin clays and loams. As a result of a powerful emergency release of a gas-soil-water mixture, drilling was stopped and a funnel was formed that has remained in the bottom relief to this day (Tulapin et al., 2021). Based on the results of these works, V.N. Bondarev and co-authors (Bondarev et al., 2002) suggested that the thickness of subaqueous permafrost composed predominantly plastic frozen and of highly ice-rich Kazantsevo clays, formed an impermeable cap that blocked the migration of gas-water fluid to the surface. In the area of weakened zones (also as a result of melting of permafrost from below), the stratum of plastic frozen Kazantsevo clays was squeezed up to the surface with the formation of PLFs.

One of the possible mechanisms for the formation of icy rocks that make up the PLFs of the Pechora Sea may be the impact of thermogenic gases on bottom sediments (Melnikov et al., 1998). Upon being released from deep oil and gas generating structures and filtered into the upper layers of the section, the gas could freeze weakly cemented water-saturated rocks due to its expansion and the Joule–Thompson effect, leading to a drop in temperature in the section. The results of thermophysical calculations show (Melnikov et al., 1998) that during this process a column of ice-saturated soils with a decrease in ice content down the section is formed under the PLFs.

However, not all researchers of the Pechora Sea PLFs are inclined to associate their formation with degassing in the presence of permafrost. In particular, according to R.B. Krapivner (2007), the origin of PLFs may be due to diapirism along deep faults and mud volcanism on the surface of the bottom. He interprets the clayey ice-rich deposits exposed by boreholes according to (Bondarev et al., 2002) as vent facies of

mud volcanoes expressed in the bottom relief (Krapivner, 2007).

In the Kara Sea area, in the depth range from 5–10 to 45 m, regional survey work (high-frequency profiling, surface soil sampling) was carried out (Portnov et al., 2013), during which a relatively low occurrence of PLFs was established in this area. The height of the identified PLFs was no more than 5 m, while the diameter varied from 30–40 to 400–500 m (Serov et al., 2015). Based on the results of isotope analysis of methane from sediment cores that make up the PLFs in the southeastern (Semenov et al., 2020) and northern parts of the Kara Sea (Serov et al., 2015), it was established that the gas may have both a deep origin associated with the melting of subpermafrost and intrapermafrost gas hydrates, and a near-surface origin associated with the melting of permafrost. Since it was the gas of deep origin that was characterized by significant concentrations in the sediments, while the content of near-surface methane was low, it was suggested that the formation of PLFs was rather associated with deep fluid flow (Serov et al., 2015).

Thus, despite the fairly widespread distribution of PLFs on the Arctic shelves, there is still no generally accepted concept of the mechanism of their formation. Further study of PLFs is of interest from both applied and fundamental points of view. Thus, in areas of ongoing degassing, PLFs are a source of risk of disruption to well drilling, construction and operation of oil and gas production infrastructure. In addition, the analysis of flow rates and fluid composition in PLF development zones is important for monitoring the global impacts of climate change, the evolution of subaqueous permafrosts, and studying the Earth's deep degassing processes.

## MATERIALS AND METHODS

The morphology of PLFs and the structure of the upper part of the shelf sedimentary section in the areas of their distribution were studied during complex geological and geophysical works at sites in the central part of the Pechora Sea with an area of about 150 km<sup>2</sup> (polygon 1), in the central part of the Kara Sea with an area of about 40 km<sup>2</sup> (polygon 2) and in the western part of the Baydaratskaya Bay with an area of about 6 km<sup>2</sup> (polygon 3) (Fig. 1) The expeditionary work was carried out by the authors within the framework of the 38th (2018), 41st (2019), 49th (2020) and 52nd (2021) cruises of the R/V *Akademik Nikolay Strakhov* and the 51st (2022) cruise of the R/V *Akademik Boris Petrov* within the framework of the program “Geological, geophysical, geomorphological, and hydrophysical studies in the Barents and Kara Seas” (project head, Doctor of Geosciences S.L. Nikiforov).

To collect the data, hardware and software complex was used that included a SeaBat 8111 multibeam echo sounder; GPS, motion sensors and gyrocompass,

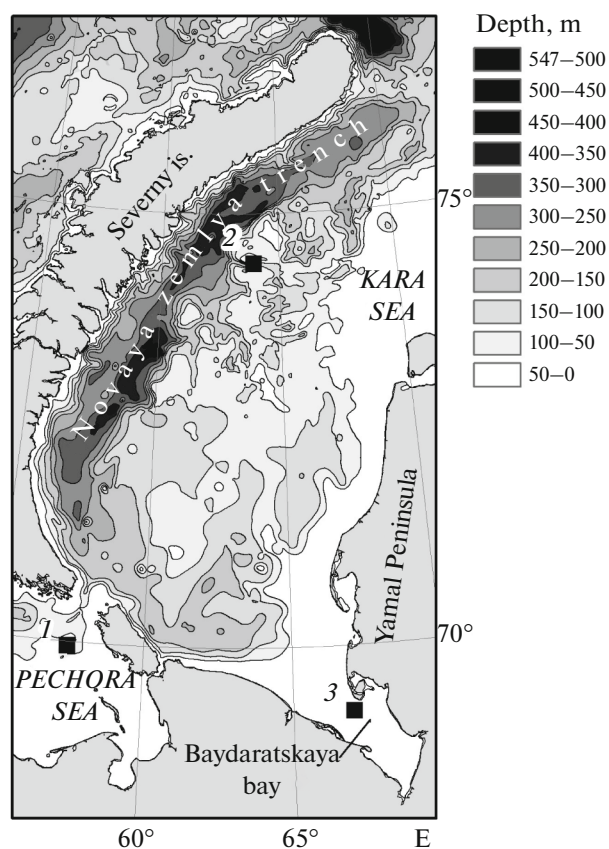


Fig. 1. The location of research sites: (1) polygon 1 (Pechora Sea); (2) polygon 2 (Kara Sea); (3) polygon 3 (Baydaratskaya Bay). The isobaths are drawn using the GEBCO digital model data ([www.gebco.net/data...](http://www.gebco.net/data...)).

combined in the Applanix POS-MV device; an SVP-70 sound velocity sensor; and an EdgeTech 3300 high-frequency acoustic profiler (resolution 0.1–1 m, acoustic signal penetration depth 10–100 m). The survey was carried out along a grid of runline (interline distance 200 m) with the simultaneous operation of multibeam echo sounder, high-frequency profiler and seismoacoustic profiling system.

At the office stage, the processing of multibeam echo sounding data was carried out in the PDS2000 software package with the creation of digital models of the bottom relief with resolution of 2 × 2 and 10 × 10 m (at polygon 1) and 10 × 10 m (at polygons 2 and 3). Using digital models of the bottom relief, the morphometric parameters of PLFs were determined: height, length, width, basal area, perimeter, and orientation (for elongated features). Calculation of statistical indicators and construction of graphs were carried out in MS Excel. Seismic data processing was carried out in the RadExPro program, and SeiSee and Kingdom Software 8.3 programs were used for interpretation and visualization. The summary analysis and interpretation of geological and geophysical data were performed in the freely distributed QGIS 3.22 package.

For use in the analysis and interpretation of the results of expeditionary research, published domestic and foreign articles on the studied issues were collected and systematized and geological, geophysical and geomorphological maps and diagrams of different scales were selected and georeferenced in a geographic information system (GIS). To analyze the relief of the surroundings of the studied polygons, the GEBCO\_2014 version 20141103 (*GEBCO\_2014...*, 2022) digital elevation model was used.

## RESULTS

**Polygon 1** is located in the outer part of the Pechora Sea shelf and is characterized by a generally flattened bottom topography. During the 38th cruise of the *R/V Akademik Nikolay Strakhov* in 2018, multibeam echo sounding and high-frequency profiling were performed at polygon 1, which made it possible to characterize the morphology and geological structure of the PLFs in high detail. In the central part of the surveyed site (see Fig. 1) there is an area of about  $5 \times 5$  km, which was studied during AMEGE works in 1988 and 1995–1996 (Bondarev et al., 2002).

Depths within the polygon vary from 47 to 82 m (Fig. 2a). It covers a gently sloping depression of the bottom with observed length of about 20 km, stretching from SSE to NNW, narrowing and bifurcating in the southeastern part of the area. Its relative depth is 25–30 m; the width along the unclear smooth edges is from 6–8 km at the southern border of the polygon to 20–25 km in the north. The territory is located at the junction of two macrofeatures of the bottom relief: the greater part is located within the abrasion-accumulative Neogene–Early Quaternary hilly-depression marine plain (depths greater than 50–55 m) with traces of pre-Late Neopleistocene sub-aerial reworking. In the southern and eastern parts, fragments of the late Neopleistocene–Holocene accumulative-abrasion plain (depths less than 50–55 m) are distinguished (Biryukov et al., 2008).

The general flattened topography of the bottom surface is complicated by 840 PLFs of isometric or elongated plan shape with shield-shaped, dome-shaped, or conical transverse profiles. PLFs are concentrated in the central and, to some extent, northern low-lying parts of the polygon and are grouped into clusters. In the eastern part of the polygon their density is maximum and reaches 35–45 units/km<sup>2</sup>; in other parts it is 20–25 units/km<sup>2</sup> (Fig. 3k). PLF heights range from 1.5–3 m to 20–25 m and the diameter (or long axis for elongated forms) ranges from 20–30 m to 300–430 m.

Based on the results of morphometric analysis of PLF, the presence of three morphological types was established (see Figs. 3, 4).

PLFs of the *first type* are located on a flat bottom. These are the largest features with a diameter of 100 to

250 m, a height of 12–15 to 20–25 m, rounded plan shape, which usually have compensatory depressions along the contour (depth from 1 to 3–4 m) (see Fig. 3a). Often, in their summit parts, there are funnels up to 1–1.5-m deep; the slopes of PLFs with a steepness from 10°–15° to 25°–35° are complicated by mudflow pseudo-terraces. The formation of clusters in the form of two or three merged or directly adjacent features without a clearly defined common base is characteristic.

PLFs of the *second type* (see Fig. 3b) are also located on a flat bottom; however, these are smaller features with a diameter from 35–50 to 120–170 m, a height from 5–7 to 10–12 m, and are rarely surrounded by compensatory depressions. The steepness of the slopes of the features does not exceed 10°–15°.

Similar to the second type of PLF, but significantly smaller, are PLFs of the *third type* (Fig. 3c). Their height is up to 5–7 m, their diameter is 100–120 m, and the slope steepness is up to 10°–15°. In some cases, adjacent PLFs merge into a single ridge-like uplift (slope steepness (10°–15°), the length of the base of which varies from 200–300 to 700–800 m; the height of the uplifts together with the base can reach 10–15 m (see Fig. 3e). In the eastern part of the polygon, in the bottom of a trough-like depression of the bottom, the density of PLFs increases noticeably, and here large oddly shaped bottom elevations with ridges built on them, as described above, and individual isometric PLFs up to 15–20 m high are observed. The steepness of the slopes of such large elevations often reaches 25°–35° (see Fig. 3d). In the central and eastern parts of the polygon, the presence of slope asymmetry and PLF elongation are noted, which is apparently associated with the accumulation of sediments transported by bottom currents from south to north (PLFs act as an obstacle to the transport of material).

The results of the morphometric analysis demonstrate a polymodal distribution of PLFs by height and the presence of three main types identified above (see Fig. 4c). The relationship between the height of the PLFs and the area of their base is close to linear (see Fig. 4a) (correlation coefficient  $r = 0.68$ ). The elongated PLFs are oriented predominantly submeridionally (azimuth 155°–225°, see Fig. 4a) and a weak relationship has been established between the height of the PLFs and their elongation coefficient ( $K_{\text{elong}}$ ): elongation is more characteristic of small features of the second and third types (see Fig. 4c).

In the eastern part of the polygon and less frequently in other parts of it, the bottom relief is complicated by pockmarks (gas springs), which are isometric closed saucer-shaped depressions with unclear edges, 1–2 m deep, and up to 70–100 m in diameter. It should be noted that, in general, pockmarks are extremely rare in areas where PLFs are distributed.

Based on the results of high-frequency acoustic profiling, three seismic stratigraphic complexes

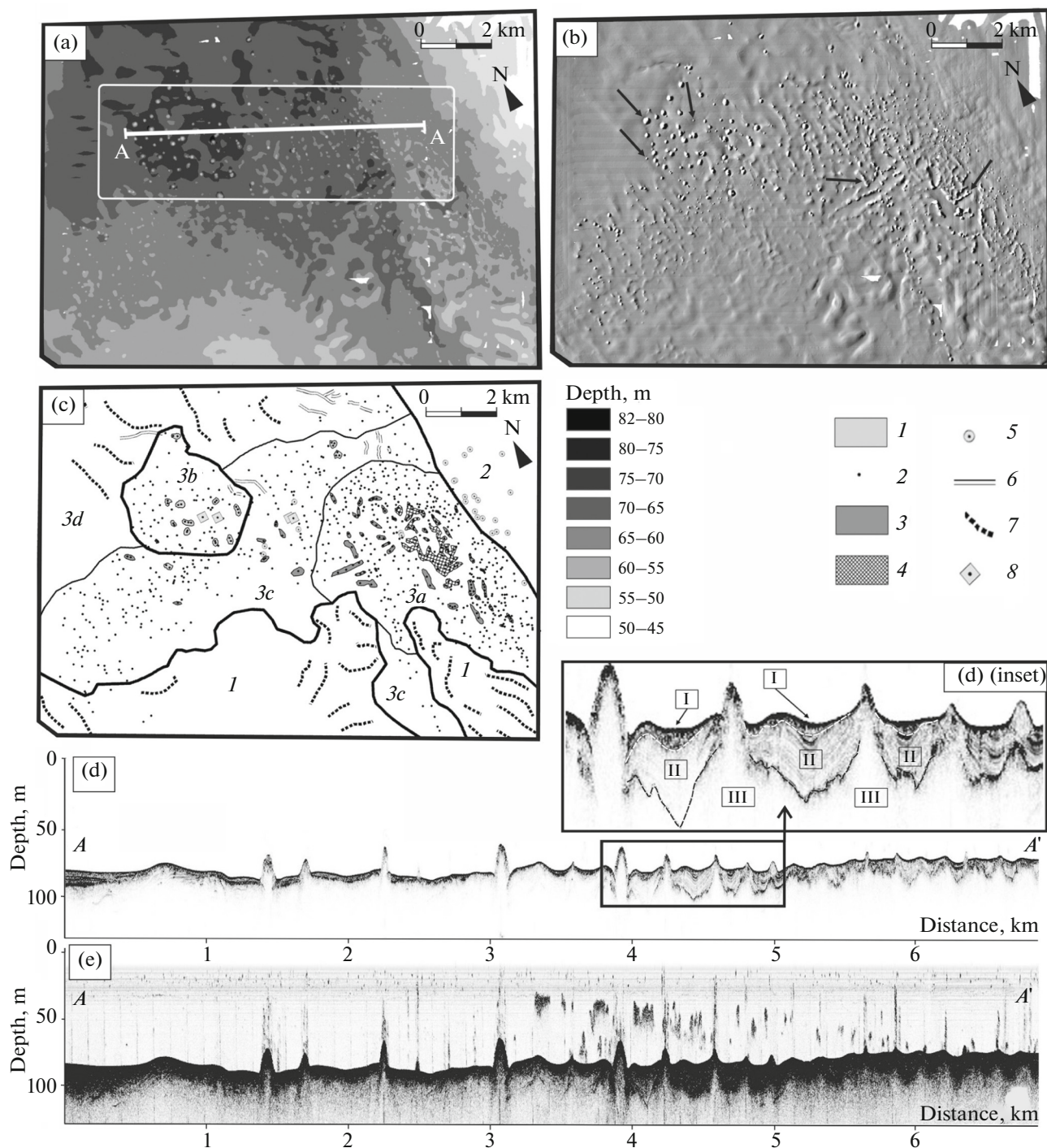


**Fig. 2.** Pingo-like features of the central part of the Pechora Sea (polygon 1): (a) a digital elevation model (based on data from the 38th cruise of the R/V *Akademik Nikolay Strakhov*, 2018; the area for which the PLFs morphometric analysis was performed is highlighted in a frame), (b) a digital model with hillshading (arrows point to the PLF, the profiles of which are shown in Fig. 3), (c) a scheme for zoning the territory based on PLFs morphology (the numbers indicate the numbers of geomorphological regions and subregions mentioned in the text), (d) a profile obtained by high-frequency acoustic profiling along line A–A' (I, II, III are seismostratigraphic complexes mentioned in the text), (e) the same, with the use of software amplification. Legend: (1) groups of PLFs of the first type; (2) individual PLFs of different types; (3) ridge-like features formed by the merging of several PLFs; (4) large massifs formed by the merging of several PLFs; (5) pockmarks; (6) channels formed by currents; (7) axes of swell-like bottom uplifts; (8) wells drilled at the site according to data from (Bondarev et al., 2002).

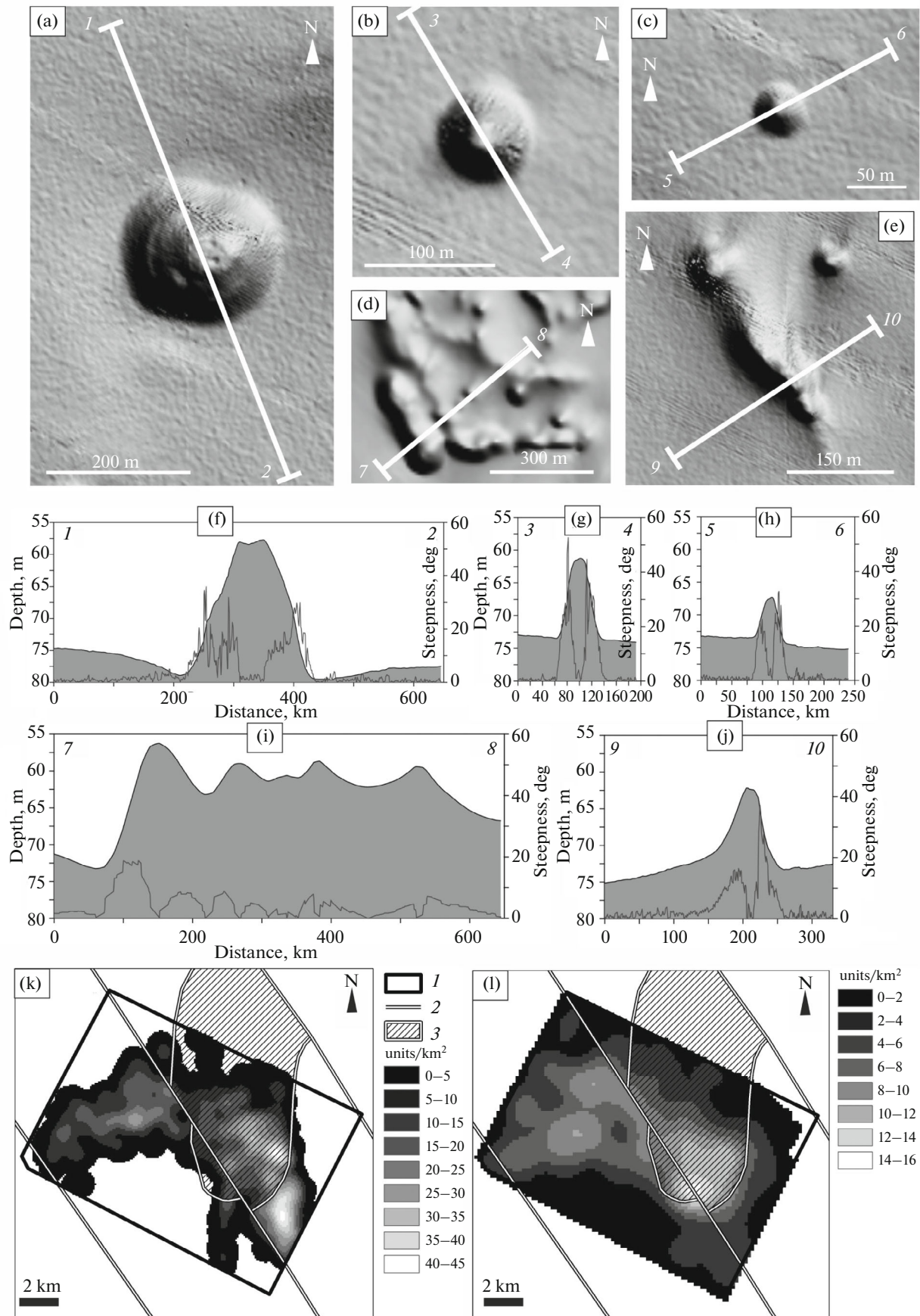


**Fig. 3.** PLFs structural types: (a) first; (b) second; (c) third; (d) massif formed by the confluence of PLFs; (e) ridge formed by the confluence of PLFs; (f–j) transverse profiles through PLFs (the line on the profiles shows the steepness of the surface); (k) density of PLFs at polygon 1; (l) density of gas manifestations in water at polygon 1. Legend: (1) boundaries of polygon (1, 2) faults (according to the data of the GGK (Viskunova et al., 2003)), (3), boundaries of the Reinekskaya prospective oil- and gas-bearing structure (according to the GGK (Viskunova et al., 2003)).

(SSCs) were identified in the bottom structure (see Fig. 2d (inset)), consistent with the stratigraphic scheme of the polygon proposed in (Bondarev et al., 2002):

(1) SSCI, which lies on the surface with a chaotic high-amplitude record with a thickness of 1–2 to 15–

25 m (marine Holocene and/or late Neopleistocene (Sartan) loams ( $mQ_3^4-Q_4$ );

(2) the acoustically layered SSCII with a thickness from 5–10 to 20–25 m (alluvial-marine late Neopleistocene (Sartan) sands and loams ( $amQ_3^4$ );

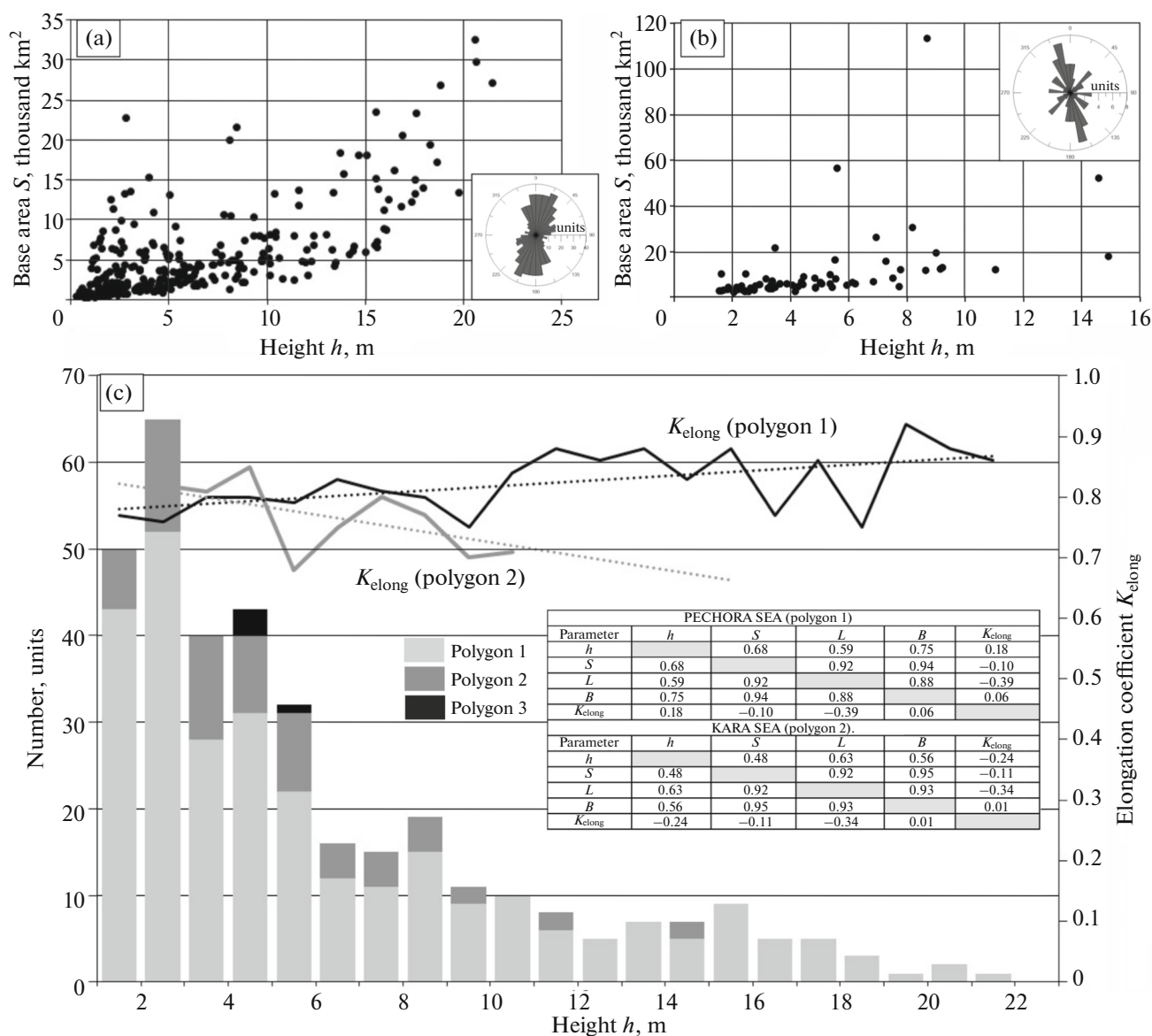


**Fig. 4.** The results of the analysis of morphometry of pingo-like features in the Pechora and Kara seas: (a) the relationship between the base area and the height of the PLFs at polygon 1 and a rose diagram illustrating the orientation of the elongated PLFs; (b) the relationship between the base area and the height of the PLFs at polygon 2 and a rose diagram illustrating the orientation of the elongated PLFs; (c) the number of PLFs of different heights at the three surveyed sites. The table shows the correlation coefficients between the main morphometric characteristics: height (*h*), base area (*S*), length (*L*), width (*B*), coefficient of elongation ( $K_{elong} = B/L$ ).

(3) the acoustically opaque SSCIII, whose roof is a complexly constructed system of reflections of various geometries and has a complex relief (associated with the roof of frozen late Neopleistocene (Kazantsev) clays and loams with high ice content ( $mQ_3^{1-3}$ ).

The SSCI deposits are located in depressions in the vicinity of the PLF and form a mantle-like cover over the uneven topography of the SSCII roof. In the western part of the polygon, where the density of PLFs decreases or they are absent, the SSCI thickness reaches 20–25 m. In the eastern part of the polygon, SSCI deposits are observed as separate packs on the bottom with a thickness of up to 1–5 m. SSCII deposits are widespread throughout the polygon and are not found only under the PLFs themselves. These sediments cover the uneven relief of the SSCIII roof surface with high-amplitude (from 4–5 to 35–40 m below the bottom) roof topography. SSCIII deposits are exposed on the bottom, comprising PLFs of different morphological types from the surface (see Fig. 2d).

Based on the results of high-frequency seismoacoustic profiling 1608 acoustic anomalies were identified, mainly associated with areas of PLF distribution on the seabed. Vertical anomalies such as gas flares are associated with the summit surfaces and slopes of the first type of PLFs (see Fig. 2e). For other PLF types, acoustic anomalies in the water column were identified as scattered chaotic structures both above the features themselves and between them. Gas manifestations in the central part of the territory are confined to areas with a high density of PLFs of the first type; the density of acoustic anomalies in the water column here reaches 5–7 pcs/km<sup>2</sup> (see Fig. 3i). In the eastern part of the polygon, where PLFs of the third type and PLF massifs are combined, the density of anomalies increases to 12–14 pcs/km<sup>2</sup>.

The identified patterns allow us to distinguish three areas within the polygon that differ in the listed parameters (see Fig. 2b).

**Region 1** covers the elevation in the southern part of the test site. Morphologically, it is a gentle (less than 2°), in places gently undulating, scarp of the late Neopleistocene–Holocene accumulative-abrasion plain. The depth is 55–65 m. PLFs and gas manifestations in the water are practically not found here. From the bottom surface, SSCI deposits with a thickness of 2–3 to 5–7 m lie almost everywhere in the form of a cover. Uplifts of the SSCIII roof, located at depths from 5–10 to 20–25 m, are traced fragmentarily.

**Region 2** is a gentle ledge (2°–3°) of the late Neopleistocene–Holocene accumulative-abrasion plain in the eastern part of the polygon. The depth is 47–65 m. The bottom relief is complicated by pockmarks located at the foot of the ledge. Near the foot of the ledge, a few gas manifestations found in the water column are grouped. At the same time, there is no spatial relationship between gas manifestations and pock-

marks. Within region 2, SSCIII deposits occur at depths of up to 5–7 m beneath a thin cover of predominantly SSCII and SSCI lenses. The roof of SSCIII is relatively level.

**Region 3** occupies the greater part of the polygon and is confined to the flat surface of the marine Neogene–Early Quaternary plain with depths from 55–60 to 75–80 m. This is the main area of development of PLFs and gas manifestations in the water column. Based on PLF density and morphology, Region 3 can be further divided into several sub-regions.

*Subregion 3a* has a depth of 60–65 to 75–77 m and shows the presence of all types of PLFs and their massifs (their density reaches 35–45 pcs/km<sup>2</sup>). The density of acoustic anomalies associated with degassing is maximum and reaches 10–15 pcs/km<sup>2</sup>. SSCIII deposits occur at shallow depths and are often exposed at the surface, forming PLFs of different types. In the depressions they occur at depths of up to 30–45 m, which creates a high contrast in the relief of the SSCIII roof within this subregion.

*Subregion 3b* is confined to the deepest part of the polygon's macro-depression (depth reaches 80–82 m). The majority of the largest PLFs of the first type are concentrated here (relative heights up to 25 m, diameters up to 250 m, and densities up to 25–40 pcs/km<sup>2</sup>). PLFs are often surrounded by compensatory depressions with a width of up to 100–120 m along the edges and a relative depth of up to 2–3 m. Compensatory depressions are characterized by slope asymmetry: steeper (10°–15° versus 2°–4°) sides face the PLF. Gas manifestations concomitant with PLF are noted, but their density is relatively low (6–10 pcs/km<sup>2</sup>). The top of the SSCIII deposits is found at depths of up to 35–40 m and is traced fragmentarily in the basins separating the PLFs. The depressions between the rises are filled with a layer of SSCI sediments up to 20–25-m thick and SSCII sediments up to 10–15-m thick.

*Subregion 3c* is located between areas 3a and 3b, the depths within the polygon boundaries vary from 55–60 to 70–75 m. All types of PLFs are found here, including ridge-shaped rises. The PLF density varies from 7–10 to 16–25 pcs/km<sup>2</sup>. The density of acoustic anomalies in the water column is from 4 to 10 pcs/km<sup>2</sup>. The SSC section within the polygon boundaries is most clearly traced. In the western and central parts of the subregion, SSCI is present almost everywhere on the surface. The top of the SSCII deposits occurs at depths from a few meters to 8–12 m. The top of the SSCIII deposits can be traced almost everywhere; it occurs at depths of up to 15–25 m and rises to the bottom surface, forming the PLF.

*Subregion 3d* is located in the northern part of the polygon. PLFs of the first and second types are rare, gas manifestations in the water column are distributed relatively evenly over the area of the sub-region; their

density is 1–4 pcs/km<sup>2</sup>. The thickness of SSCI sediments is maximum at the polygon and reaches 30–35 m. In the eastern part of the subregion, SSCII deposits are exposed on the bottom surface. The top of the SSCIII deposits in the sub-region is traced fragmentarily at depths greater than 50–65 m and rises to the bottom surface, forming the PLFs.

**Polygon 2** is located in the western part of the Kara Sea, near the eastern edge of the Novaya Zemlya Trench, within the contours of the Universitetskaya-1 oil and gas structure at depths from 46 to 110 m (see Fig. 1). Multibeam echo sounding and high-frequency seismic profiling were carried out during cruise 49 of the R/V *Akademik Nikolay Strakhov* (2020) and cruise 51 of the R/V *Akademik Boris Petrov* (2022). Along the boundaries of the polygon there are uplifts, outlined by 45–50 m isobaths, and in its central part there is a submeridional depression with depth marks in the axial part of about 70–110 m (Fig. 5a). Judging by the morphology and plan shape, the negative macrofeatures of the polygon's topography are fragments of ancient (apparently Neogene (Lastochkin, 1984)) valleys, largely reworked by fluvio-glacial processes in the Pleistocene. The most deep parts of the bottom of the central paleovalley are characterized by a flattened or slightly undulating relief and the presence of local depressions with depths of up to 100–110 m. Asymmetrical uplifts up to 20–25-m high adjoin the depressions. One side of uplifts is usually steep (up to 15°–20°) with a clearly defined edge, the second is smoothed (up to 5°–7°). There is no pattern in the distribution of exposure of steep and gentle slopes of uplifts. Often the uplifts have scalloped edges in plan and a chaotic dissected relief, which allows us to assume that the processes of slumping and sliding participated in the formation of their appearance. The complex of these features forms the general hilly-depressed appearance of the bottom of the paleovalley.

According to the G GK sheet S-41-43 (Kostin et al., 2004), the surface of the bottom in the area of work is covered by Holocene marine silts and glaciomarine late Neopleistocene deposits, represented by loams, sandy loams and clays up to 20–25-m thick. Below, silty clays of the Eocene and Oligocene–Miocene up to 70–100-m thick lie, interpreted as deltaic deposits (Kostin, 1998).

On gentle slopes and to a lesser extent in the bottom of the paleovalley, PLFs are widespread (57 were identified) (see Fig. 5). These are rounded dome-shaped structures, on average up to 100 m in diameter, up to 5–7-m high, with slopes no steeper than 15°. Single PLFs have much more impressive dimensions and a shield-shaped cross-section, their height is up to 25 m, their diameters are 450–500 m, the steepness of the slopes is not great, up to 8°–10°, and on the summit surface there are funnel-shaped depressions up to 3 m deep and up to 50–80-m in diameter. When conducting morphometric analysis, the largest PLFs, appar-

ently formed earlier by the merger of smaller ones, were not taken into account. Just as at polygon 1, PLFs of the third type with a height from 2–3 to 6–7-m dominate here (see Fig. 4c). At the same time, the direct relationship between the height and the area of the PLF base is significantly weaker (see Fig. 4c,  $r = 0.48$ ), which may be associated, among other things, with the greater age of the features. In general, the few elongated PLFs are oriented submeridionally (azimuth 145°–185°, see Fig. 4b), and the elongation of the PLFs increases with increase of their height (see Fig. 4c). This change in morphology may be associated with the influence of bottom currents. Moreover, unlike polygon 1, large PLFs here are composed of partially or completely thawed rocks from the surface, so the fine sediment that makes them up is apparently involved in the bottom transport, which leads to the appearance of an elongated shape.

The surfaces of gentle elevations of the bottom are complicated by rare pockmarks up to 100–150-m in diameter, up to 2–3-m deep. On the slopes of the paleovalley, areas of chaotic microrelief with ridge features oriented both parallel to the slope and across it are widely developed. The relative differences in elevation in such areas are 5–6 m, the distance between the ridges does not exceed 15–30 m, and the steepness of the ridge slopes reaches 15°–20° or more. Judging by the morphology and geomorphological position of these ridges, their genesis may be associated with the processes of landslides and slumping of sediments on the slopes of the paleovalley. The flattened summit surfaces of the uplifts surrounding the ancient valley are complicated by iceberg gouges 30–150-m wide and 2–10-m deep. The gouges usually end on the slopes of the uplifts, but the longest gouge in the central part of the polygon can be traced from the edge to the bottom (to depths of about 90 m).

In sections obtained using the high-frequency seismic acoustic profiling method, it is not possible to trace extended reflecting horizons, with the exception of the base of the seismic complex with a layered acoustic appearance up to 20–22-m thick (see Fig. 5d). This seismic complex can be interpreted as a layer of marine Quaternary deposits, represented by marine Holocene and glaciomarine late Neopleistocene silts, loams, sandy loams and clays (mQ<sub>4</sub> + gmQ<sub>3</sub>). Further down the section, the acoustic signal is absorbed, or individual randomly located reflecting horizons associated with deltaic Eocene and Oligocene–Miocene clays can be traced. Based on the acoustic appearance, three types of sections can be distinguished within the surveyed area (see Figs. 5c, 5d, 5e):

(1) a section represented by an acoustically layered pack of supposed Quaternary deposits from the surface (mQ<sub>4</sub> + gmQ<sub>3</sub>) and an acoustic basement in the form of supposed pre-Quaternary deposits;

(2) acoustically practically impermeable stratum from the bottom surface;

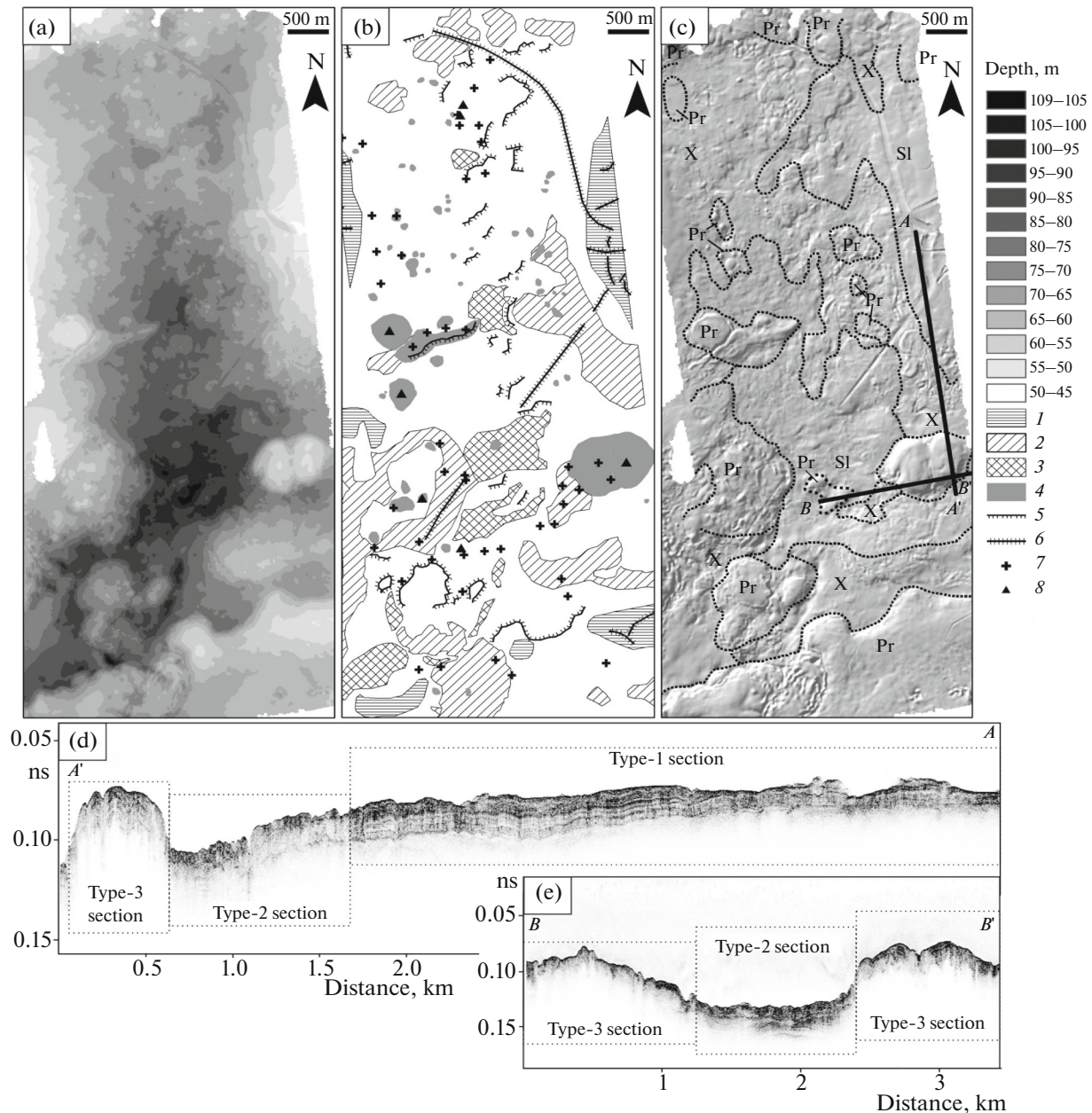


**Fig. 5.** The morphology of the bottom relief and structure of the PLFs at polygon 2 (Kara Sea). (a) Digital elevation model (based on data from the 49th cruise of the R/V *Akademik Nikolay Strakhov*, 2020); (b) structure of the bottom mesorelief; (c) types of bottom acoustic section (Sl, layered (1 type); Pr, impermeable (type 3); X, chaotic (type 2)); (d, e) profiles obtained by seismo-acoustic profiling along lines A–A' and B–B'. Legend: (1) flattened elevations; (2) hilly areas with chaotic mesorelief; (3) depressions; (4) pingo-like features; (5) edges of asymmetrical uplifts; (6) exaration furrows; (7) gas manifestations in water; (8) pockmarks.

(3) a section combining small layered packs, local reflecting areas and completely acoustically transparent areas, with reflections and layering recorded within negative and acoustically opaque areas within positive features of mesorelief.

The first type of section is characteristic mainly of depressions in the axial part of a valley-like depression and areas of large uplifts to the west and east (paleo-interfluvial) (see Fig. 5c). The second type of section is

typical for PLFs. The acoustic impermeability observed locally in this type of sedimentary strata section may be caused by the presence of permafrost rocks (their distribution over the test site area has been confirmed by drilling (Mironyuk et al., 2019)). The third type of section is typical for areas with chaotic mesorelief on the gentle slopes of the paleovalley and most of the asymmetric uplifts at the bottom of the paleovalley. Chaotic reflections and the generally complex seismic appearance of the section in these

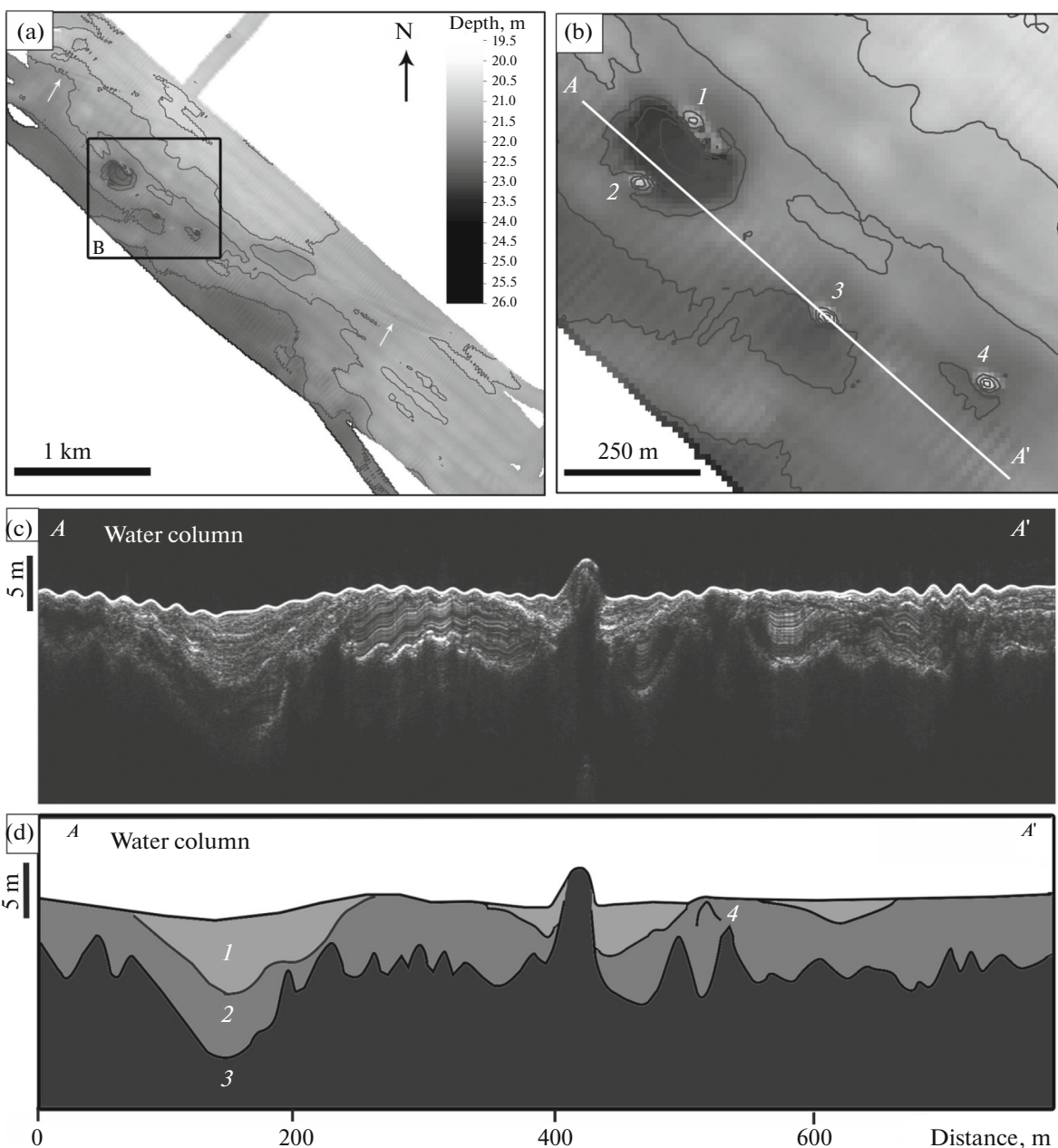


**Fig. 6.** Relief morphology and PLFs structure at polygon 3 (Baydaratskaya Bay): (a) digital elevation model (according to data from the 52nd cruise of the R/V *Akademik Nikolay Strakhov*, isobaths are drawn every 0.5 m, arrows show exaration grooves); (b) digital model of the area of polygon 3, complicated by PLFs (A–A', position of the seismoacoustic section); (c) section obtained by the high-frequency acoustic profiling method; (d) the same, with interpretation ((1) SSC I; (2) SSC II; (3) SSC III); (4) forming PLF).

areas may be due to a combination of frozen and thawed sediments within positive and negative relief features, respectively.

Gas manifestations in the water column (see Fig. 5b) are mainly confined to areas with chaotic bottom relief, pockmarks and PLFs and most often represent poorly detectable areas of increased acoustic turbidity. Vertical flare-type acoustic anomalies are extremely rare and are associated only with the largest PLFs.

**Polygon 3** is located in the central part of the Baydaratskaya Bay of the Kara Sea, 12 km southwest of Cape Ponton, the southern end of the Maresalskie Koshki spit (see Fig. 1); the depth varies from 19 to 26 m. The eastern part of the polygon is located at depths of 21–22 m, while the western part is relatively low (depths of 23–24 m) (Fig. 6a).

The bottom relief within the polygon is stepped with a general slope from northeast to southwest, and

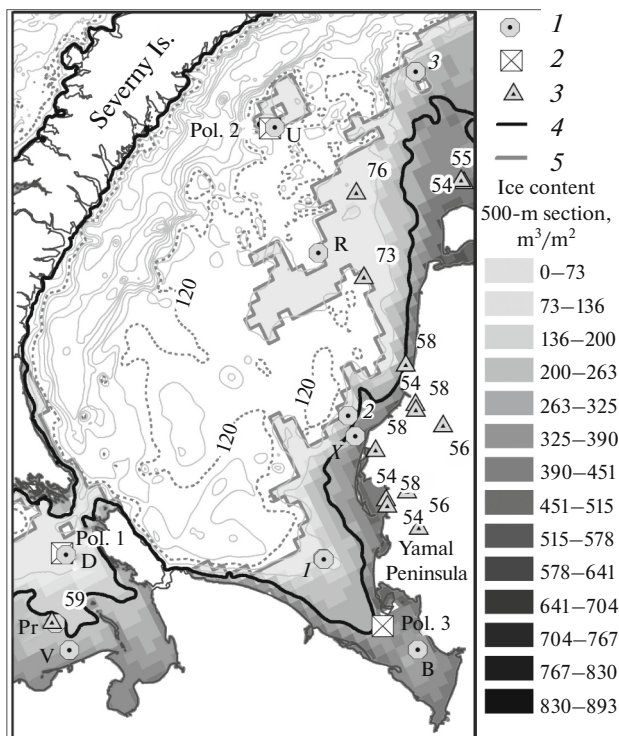


**Fig. 7.** The state of knowledge and model ice content (according to (Overduin et al., 2019)) of permafrost rocks. Legend: (1) wells that have uncovered permafrost (letters indicate the surveyed areas, see Table 1, according to (Melnikov and Spesivtsev, 1995; Bondarev et al., 2002; Kamalov et al., 2006; Serov et al., 2015; Mironyuk et al., 2019)); (2) polygons considered in this paper; (3) heat flow measurement points and its value in  $\text{mW}/\text{m}^2$  (according to (Khutorskoy et al., 2003)); (4) 20-m isobath (according to GEBCO model); (5) permafrost distribution boundary according to (Overduin et al., 2019) model.

represents a marine plain of late Neopleistocene age, formed during the Kargininskaya transgression (Nazarov et al., 2015). In the northern and north-eastern parts of the polygon, the bottom surface is complicated by ice gouges with a depth of about 0.5 m and a width of up to 45–50 m. In the central part of the polygon, five slightly elongated PLFs with a height of about 3–4 m, a width of 40–45 m, a length of 50–70 m with symmetrical slopes with a steepness of  $8^\circ$ – $12^\circ$  were identified.

According to the results of high-frequency seismic-acoustic profiling, no pronounced gas manifestations were found in the water column, however, signs of gas saturation of sediments are visible in sections with three seismostratigraphic complexes associated with SSC, identified for the central part of Baydaratskaya Bay in the work (Rokos and Tarasov, 2007) (Fig. 6):

(1) SSC I lying on the surface with a chaotic high-amplitude record with a thickness from a few meters to 10–15 m (associated with marine Holocene silts and sands, loams ( $\text{mQ}_4$ )); the deposits are located in local depressions in the relief and in the roof depressions of

the underlying horizon; their thickness and area of distribution increase in the southern direction with increasing bottom depths;

(2) acoustically layered, gas-saturated SSC II with a thickness of 3 to 7 m (associated with Kargininsky clays and loams ( $\text{mQ}_3$ )); lies mainly under the SSC I, in the northern and southern parts of the polygon it is often exposed on the bottom surface;

(3) acoustically opaque SSC III with dissected roof relief (associated with the roof of frozen and/or gas-saturated Zyryan sands ( $\text{amQ}_3$ )); on the surface of the bottom, SSC III deposits are exposed only directly on the PLFs themselves, which they compose.

A special feature of the PLF polygon is their best morphological expression and frequent proximity to fairly deep depressions. In particular, the slightly elongated uplifts in the northern part of the polygon (1 and 2, see Fig. 6b) have a height of about 2–2.5, a width of 35 to 40, and a length of 55–60 m. They are separated by a depression with elongated plan shape, 100–120-m wide and 210–220-m long, with a slope steepness of  $16^\circ$ – $18^\circ$  and a relative depth of about 5.5 m. The depression is filled with SSC I deposits up to 15-m thick (see Figs. 6c, 6d). PLFs in the southeastern part of the polygon (3 and 4, see Fig. 6b) have similar morphometric parameters (height about 3, width about 35, length about 70 m). They are surrounded by depressions up to 1-m deep and about 200 m in diameter and filled with SSC I deposits up to 9–11-m thick. Acoustic anomalies are often recorded in the thickness of SSC II sediments, in particular, bright spots in areas close to the surface of the SSC III roof. An anomaly of this kind was found on the southern side of a large depression in the central part of the polygon (shown as number “4,” see Fig. 6d). It can be assumed that the formation of a new PLFs is beginning in the brow part of this depression.

## DISCUSSION OF THE RESULTS

An analysis of the results of previous PLF studies (Portnov et al., 2013; Serov et al., 2015; Bogdanov et al., 2002) and new data obtained on the southwestern part of the Kara shelf and the central part of the Pechora Sea shelf allows us to conclude that the morphology of PLFs and their modern dynamics are determined by a set of conditions and factors of the development of the shelf zone. In particular, the obtained data confirm that PLF areas on the shelf are confined to areas of permafrost occurrence and are associated with areas of degassing both in the water column and in the loose sediments that make up the bottom. The presence of permafrost rocks at different depths (from 10–20 to 40 m) in the upper part of the sedimentary section of the southwestern part of the Kara shelf has been repeatedly confirmed by drilling (Fig. 7, Table 1) and seismic profiling.

**Table 1.** The depth of the roof of permafrost rocks in the Pechora and Kara seas (southwestern part) according to published data

Area*	Source	Sea depth, m	The permafrost roof depth, m from bottom surface
Axial part of Baydaratskaya Bay (B)	Kamalov et al., 2006	20–25	10–20
Prirazlomnaya site (Pr)	Melnikov and Spesivtsev, 1995	21	22.5
Varandeykaya site (V)		15	40
Pechora Sea, Diapiry polygon (D)	Bondarev et al., 2002	58–72	From 0 (on PLF) to 25–30
Rusanovskaya site (R)	Melnikov and Spesivtsev, 1995	114	13.5
		80	10
University site (U)	Mironyuk et al., 2019	75–80	5–10
Baydaratskaya Bay Throat (1, location of drilled PLF)	Serov et al., 2015	35	0 (on PLF)

\* For letter designation see Fig. 7.

Acoustic markers of the presence of permafrost in the south and southeast of the Kara shelf have been identified to depths of about 60–70 m, with its roof established at a depth of 5–60 m (mostly 10–20 m) from the bottom surface (Rekant and Vasiliev, 2011). At the same time, the authors (Rekant and Vasiliev, 2011) note that permafrost can potentially be found at depths greater than 60–70 m.

These studies confirm the presence of signs of degassing in the areas of PLF distribution, as noted in earlier works (Paull et al., 2007; Serov et al., 2015; Mironyuk et al., 2019; Mironyuk, 2020). It was previously indicated (Portnov et al., 2013) that the majority of gas show areas are concentrated in areas with bottom depths greater than 20 m; at shallower depths, degassing is impeded by the presence of continuous permafrost. Moreover, the presence of methane at depths of about 45 m, probably associated with the influx of groundwater from land along the permafrost base (Semenov et al., 2020), indicates the possible spread of continuous permafrost at greater depths.

The results of mathematical modeling of the conditions for the existence of the permafrost layer on the shelf (Portnov et al., 2014) show the following characteristics of the permafrost at a model depth of 40 m: with a heat flow of about 50 mW/m<sup>2</sup> permafrost thickness reaches about 170–200 m, at 60 mW/m<sup>2</sup> the permafrost thickness is reduced to 70–80 m. With a heat flow of 70 mW/m<sup>2</sup> the compact layer of frozen rocks is replaced by separate thin (less than 30–40 m) permafrost islands. With decreasing sea depth, the thickness of the permafrost layer and its continuity increase, while the depth of the roof decreases (Portnov et al., 2014). At the same time, according to modeling data from other authors (Gavrilov et al., 2020), the thickness of the permafrost on the shelf does not exceed 100 m, and at sea depths of more than 20 m continuous permafrost and large insular massifs of frozen

rocks are completely absent. Other model estimates indicate the possibility of much thicker (350–500 m) permafrost strata on the shelf (Overduin et al., 2019). At the same time, the model (Overduin et al., 2019) indicates a wider distribution of insular permafrosts, although at depths greater than 40–50 m, the ice content of permafrosts decreases sharply according to the modeling results (see Fig. 7). At the same time, model calculations do not take into account local inhomogeneities in soil characteristics (for example, actual fluctuations in ice content) and increased heat flow values associated with faults and fracture zones. Therefore, it is impossible to exclude the presence of permafrost massifs of significant thickness and area in the depth range from 20–30 to 110–120 m. Some studies indicate the possibility of the spread of sporadic permafrost at greater depths (up to 250 m and more, according to (Shpolyanskaya, 2015)).

Using the modeling results (Overduin et al., 2019; Gavrilov et al., 2020), published information (see references in Table 1) and our own materials on key research sites, we can assume that, taking heat flow values of about 60–75 mW/m<sup>2</sup> into account in the considered water area of the Kara and Pechora seas, the thickness of subaqueous permafrost apparently does not exceed 100 m. At the same time, continuous permafrost is present in shallow waters down to depths of about 20–30 m. At greater depths, permafrost is distributed in the form of separate insular massifs; at depths from 70–80 to 100–110 m, their presence has not been reliably established.

Thus, the development of the bottom relief of the studied areas of the shelf occurs in complex geocryological conditions and under the influence of the degassing process, the nature of which in different parts of the shelf zone remains controversial. PLFs undoubtedly owe their origin to the complex interaction of fluids rising to the surface of the bottom with

the geocryologically and lithologically heterogeneous stratum of rocks that make up the bottom. The results of these studies allow us to conclude that the density and morphology of PLFs in different parts of the shelf are largely related to the history of shelf development over the past 10000–15000 years, which, in turn, determined the differences in the thickness and nature of permafrost, as well as the intensity of degassing at present.

Polygon 3 (Baydaratskaya Bay) is located in an area of continuous permafrost rocks on the shelf. The transgression began here about 7000–8000 years ago (Gavrilov et al., 2020) and apparently occurred at a fairly high speed. At the same time, the phase of the flooded land being located in the zone of wave action and immersion to depths of maximum water heating of about 5–10 m did not last long; permafrost thawed to a shallow depth, below which the rock temperature remained negative (Kamalov et al., 2006). Despite the relatively low intensity of ice gouging in the depth range of more than 15–20 m (Ogorodov, 2014), polygon 3 should have been subject to exaration for at least the last 5000–6000 years (Gavrilov et al., 2020). At the same time, the absence of any signs of ice influence in the microrelief of the summit surfaces and slopes of the PLFs was revealed. Thus, it can be concluded that the PLFs at the bottom of the Baydaratskaya Bay are relatively young fluidogenic features formed by squeezing out plastic frozen (and in places partially thawed) rocks under the action of fluid flow. The absence of manifestations of degassing in the water column and pronounced vertical anomalies in the section of thawed rocks indicates, in general, a weak intensity of degassing at the bottom surface. This is probably due to the presence of continuous permafrost, which acts as a fluid seal.

At polygon 2 (Kara Sea) with depths of 100–110 m, the environment of the most ancient onset of marine conditions at the turn of the late Neopleistocene and Holocene is observed. Permafrost degradation began here in the early stages of the transgression about 12000–15000 years ago (Gavrilov et al., 2020) and apparently the formation of individual PLFs also began at the same time. The development of PLFs occurred in conditions of fairly active bottom currents, which led to the manifestation of asymmetry in their morphology. The processes of permafrost degradation were accompanied by both area thawing and slumping, as well as solifluction on the slopes of the paleovalley, which led to the formation of a hilly-depressed surface of its bottom and a ridge-like relief on the slopes. Apparently, it is precisely the partial thawing of the rocks that make up the PLFs and their displacement along the slopes of these features that is associated with the weakness of the relationship between the height of the PLFs and the area of their base, as established during the morphometric analysis. It can be concluded that the formation of new PLFs at this site by bulging of plastic soils under influence of gas pres-

sure on the permafrost base is currently practically no longer occurring or is not occurring at all (permafrost have most likely degraded, since it cannot be confidently identified on acoustic sections). The previously formed PLFs are currently developing under the influence of slope processes (traces of mass landslides have been noted on their slopes), as well as the process of degassing along vertical channels, clearly visible on the profile (see Figs. 5d, 5e). It is possible to assume some participation of pseudovolcanism in the modern dynamics of large PLFs; this possibility was indicated in (Mironyuk et al., 2019).

The territory of polygon 1 (Pechora Sea) was flooded during transgression about 10000–12000 years ago (Gavrilov et al., 2020). By this time, a thick layer of alluvial-marine and lake deposits had formed here, which was largely frozen. Apparently, the combination of the great thickness of Quaternary deposits (including permafrost), high degassing activity and the presence of a fault system (possibly active at the present stage (Krapivner, 2007)) led to the formation of a large number of PLFs of different morphological types. The areas of maximum density of gas shows and PLFs correlate well with the faults and contours of the Reinekskaya oil- and gas- bearing structure, established at the test site according to data from (Viskunova et al., 2003) (see Figs. 3k, 3l). The presence of crater-like depressions on the summits and landslide features on the slopes of the PLF, ridge-like uplifts, coupled with the almost ubiquitous development of gas manifestations on large PLFs indicate a very high modern activity of heaving processes. Thus, in the central part of the Pechora Sea, the formation of PLFs occurred quite a long time ago and the process of heaving under the influence of fluid flow continues to this day. The orientation of the ridge-like uplifts formed by the merging of closely located PLFs in polygon 2 shows orthogonality (see Fig. 2c), which can be explained by the squeezing out of plastic soils along interblock depressions of degrading permafrost with a polygonal-vein structure.

These results demonstrate the dependence of the morphology and modern dynamics of the fluidogenic relief of the shelf on the geological and tectonic position, the presence and nature of permafrost, the intensity of degassing, as well as the time of flooding of a specific section of the shelf during the Holocene transgression. Moreover, the initial conditions for the formation of permafrost in the PLF section could have been either submarine (throttling effect (Melnikov et al., 1998), freezing of fresh subpermafrost groundwater upon contact with cold bottom waters (Serov et al., 2015; Paull et al., 2022)) or subaerial (Bondarev et al., 2002; Paull et al., 2007). Whatever the mechanism of permafrost formation, the origin of PLFs on the shelf can be confidently associated with the swelling and squeezing of rocks under the action of fluid flow from the subsurface. It is noteworthy that such

features have not yet been discovered outside the areas of permafrost occurrence.

## CONCLUSIONS

Based on the presented research results, the following main conclusions can be formulated, which supplement existing ideas (Bondarev et al., 2002; Mironyuk et al., 2019; Paull et al., 2022; Portnov et al., 2013; Serov et al., 2015) about the nature of the distribution and dynamics of PLFs on the shelves of the Western Arctic seas.

(1) PLFs were formed in subaqueous conditions after shelf flooding during the Holocene transgression as a result of bulging and squeezing of plastic ice-bearing rocks under the action of fluid flow from the subsurface. The density and morphological diversity of PLFs depend on the geological and tectonic position of the bottom area, the presence and nature of permafrost, the intensity of degassing, and the time of shelf flooding during the Holocene transgression.

(2) In areas with depths greater than 70–80 m, these features were formed in the early stages of the Holocene transgression; the permafrost there has already thawed to a significant extent and in some places completely. However, PLFs retain their expression in the relief and are actively transformed by the activity of bottom currents, slope and, possibly, pseudo-volcanic processes associated with ongoing degassing.

(3) In shallow (up to 20–30 m) areas of the shelf close to the shore, PLFs are not common and apparently continue to form at the present time. At the same time, the high thickness and continuity of permafrost prevent active fluid flow, and gas shows in water and the loose part of the upper sedimentary section are relatively few in number. PLFs of such areas have the morphology of cone-shaped knobs and the absence of signs of intensive gas release.

(4) At intermediate depths (from 20–30 to 70–80 m), in the presence of insular or discontinuous permafrost under conditions of high fluid flow intensity in the area of fault zones and perspective oil- and gas-bearing structures, the morphological diversity and density of PLFs reach maximum values. In such areas, ongoing heaving processes and active degassing are combined in the near-surface sedimentary layer, which determines the wide variety of morphological types of PLFs.

## FUNDING

Marine expeditionary work was carried out within the framework of the state task of the GIN RAS No. FMUN-2019-0076 “Geological hazards in the World Ocean and their relationship with the relief, geodynamic and tectonic processes” (2018–2021), as well as on the topic of the state task of the IO RAS FMWE-2021-0005. Expeditionary

studies in 2022 and their office processing were supported by the Russian Science Foundation project no. 22-77-10091 “Spatial Patterns of Degassing Manifestations on the Barents-Kara Shelf and Its Influence on the Relief and Bottom Sediments.”

## CONFLICT OF INTEREST

The authors of this work declare that they have no conflicts of interest.

## REFERENCES

- Biryukov, V.Yu., Ermolov, A.A., and Ogorodov, S.A., Bottom relief of the Baidaratskaya Bay, *Vestnik Mosk. Univ. Ser. 5: Geogr.*, 2008, no. 3, pp. 80–84.
- Bondarev, V.N., Rokos, S.I., Kostin, D.A., Dlugach, A.G., and Polyakova, N.A., Underpermafrost accumulations of gas in the upper part of the sedimentary cover of the Pechora Sea, *Russ. Geol. Geophys.*, 2002, vol. 43, no. 7, pp. 587–598.
- GEBCO\_2014 Grid—version 20141103. [https://www.gebco.net/data\\_and\\_products/gridded\\_bathymetry\\_data/version\\_20141103](https://www.gebco.net/data_and_products/gridded_bathymetry_data/version_20141103) (Accessed September 1, 2022).
- Gavrilov, A., Pavlov, V., Fridenberg, A., et al., The current state and 125kyr history of permafrost on the Kara Sea shelf: Modeling constraints, *The Cryosphere*, 2020, vol. 14, pp. 1857–1873. <https://doi.org/10.5194/tc-14-1857-2020>
- Judd, A. and Hovland, M., *Seabed Fluid Flow: The Impact on Geology, Biology and the Marine Environment*, Cambridge: Cambridge Univ. Press, 2007.
- Kamalov, A.M., Ogorodov, S.A., Birukov, V.Ju., Sovershaeva, G.D., Tsvetsinsky, A.S., Arkhipov, V.V., Belova, N.G., Noskov, A.I., and Solomatin, V.I., Coastal and seabed morpholithodynamics of the Baydaratskaya Bay at the route of gas pipeline crossing, *Kriosfera Zemli*, 2006, vol. 10, no. 3, pp. 3–14.
- Khutorskoi, M.D., Podgornykh, L.V., Gramberg, I.S., and Leonov, Yu.G., Thermal tomography of the West Arctic Basin, *Geotectonics*, 2003, no. 3, pp. 79–96.
- Kostin, D.A., Miocene delta of the South Kara shelf, *Byull. Mosk. O-va Ispyt. Prir., Otd. Geol.*, 1998, vol. 73, no. 5, pp. 65–68.
- Kostin, D.A., Kuzin, I.L., and Lopatin, B.G., *Gosudarstvennaya geologicheskaya karta Rossiiskoi Federatsii masshtaba 1 : 1000000 (vtoroe pokolenie). List S-41-43. Karta pliotsen-chetvertichnykh obrazovaniy* (The 1 : 1000000 State Geological Map of the Russian Federation (2nd ed.). Sheet S-41-43. Map of Pliocene–Quaternary Deposits), St. Petersburg: Kartogr. Fabr. Vseross. Nauchno-Issled. Geol. Inst., 2004.
- Krapivner, R.B., Indications of neotectonic activity at the Barents Sea shelf, *Geotectonics*, 2007, vol. 41, no. 2, pp. 73–89.
- Lastochkin, A.N., Morphology and genesis of submarine valleys of the northern shelf of Eurasia, in *Vozrast i genezis pereuglublenii na shel'fakh i istoriya rechnykh dolin* (Age and Origin of Shelf Overdeepening and History of River Valleys), Moscow: Nauka, 1984, pp. 22–28.

- Mel'nikov, V.P. and Spesivtsev, V.I., *Inzhenerno-geologicheskies i geokriologicheskies usloviya shel'fa Barentseva i Karskogo morei* (Engineering-Geological and Geocryological Conditions of the Shelf of the Barents and Kara Seas), Novosibirsk: Nauka, 1995.
- Mel'nikov, V.P., Fedorov, K.M., Vol'f, A.A., and Spesitsev, V.I., Analysis of a possible scenario for the formation of bottom ice mounds on the Pechora Sea shelf, *Kriosfera Zemli*, 1998, vol. 11, no. 4, pp. 51–57.
- Mironyuk, S.G., Fluidogenic formations: Substantiation of the identification of a new genetic group of the seabed relief, in *VIII Shchukinskie chtenija: rel'ef i prirodopol'zovanie. Mater. Vseross. Konf. s mezhd. uchastiem* (VIII Shchukin's Readings: Relief and Management of Natural Resources. Proc. All-Russ. Conf. with Int. Participation), 2020, pp. 37–43.
- Mironyuk, S.G., Kolyubakin, A.A., Golenok, O.A., Roslyakov, A.G., Terekhina, Ja.E., and Tokarev, M.Yu., The mud volcanic structure (volcanoides) Kara Sea: Morphological features and structure, in *Geology of Seas and Oceans. Proc. XXIII Int. Conf. on Marine Geology*, Moscow: Inst. Okeanol. Ross. Akad. Nauk, 2019, vol. 5, pp. 192–196.
- Nazarov, D.V., Kostin, D.A., Shishkin, M.A., and Faibusov, Ya.E., *Gosudarstvennaya geologicheskaya karta Rossiiskoi Federatsii masshtaba 1 : 1000000 (tret'e pokolenie). Zapadno-Sibirskaya seriya. List R-42. Karta pliotsen-chetvertichnykh obrazovaniy* (The 1 : 1000000 State geological map of the Russian Federation (3rd ed.). West Siberian Ser., Sheet R-42. Map of the Pliocene–Quaternary Deposits), St. Petersburg: Kart. Fabr. Vseross. Nauchno-Issled. Geol. Inst., 2015.
- Ogorodov, S.A., Relief-forming activity of sea ice, *Doctoral (Geogr.) Dissertation*, Moscow, 2014.
- Overduin, P., Schneider von Deimling, T., Miesner, F. et al., Submarine permafrost map in the Arctic modeled using 1-D transient heat flux (SuPerMAP), *J. Geophys. Res.: Oceans*, 2019, vol. 124, no. 6, pp. 3490–3507.  
<https://doi.org/10.1029/2018JC014675>
- Paull, C.K., Lii, W.U., Dallimore, S.R., and Blasco, S.M., Origin of pingo-like features on the Beaufort Sea shelf and their possible relationship to decomposing methane gas hydrates, *Geophys. Res. Lett.*, 2007, vol. 34, L01603.  
<https://doi.org/10.1029/2006GL027977>
- Paull, C.K., Dallimore, S.R., Jin, Y.K., Caress, D.W., et al., Rapid seafloor changes associated with the degradation of Arctic submarine permafrost, *PNAS*, 2022, vol. 119, no. 12.  
<https://doi.org/10.1073/pnas.2119105119>
- Portnov, A., Smith, A.J., Mienert, J., Cherkashov, G., et al., Offshore permafrost decay and massive seabed methane escape in water depths >20 m at the South Kara Sea shelf, *Geophys. Res. Lett.*, 2013, vol. 40 (15), pp. 3962–3967.  
<https://doi.org/10.1002/grl.50735>
- Portnov, A., Mienert, J., and Serov, P., Modeling the evolution of climate-sensitive Arctic subsea permafrost in regions of extensive gas expulsion at the West Yamal shelf, *J. Geophys. Res. Biogeosci.*, 2014, vol. 119, pp. 2082–2094.  
<https://doi.org/10.1002/2014JG002685>
- Rekant, P.V. and Vasil'ev, A.A., Distribution of subaqueous permafrost rocks on the shelf of the Kara Sea, *Kriosfera Zemli*, 2011, vol. XV, no. 4, pp. 69–72.
- Rokos, S.I. and Tarasov, G.A., Gas-saturated sediments of bays and bays of the southern part of the Kara Sea, *Byull. Kom. po Izucheniyu Chetvertichnogo Perioda*, 2007, no. 67, pp. 66–75.
- Semenov, P., Portnov, A., Krylov, A., Egorov, A., and Vanshtein, B., Geochemical evidence for seabed fluid flow linked to the subsea permafrost outer border in the South Kara Sea, *Geochemistry*, 2020, vol. 80, no. 3, p. 125509.  
<https://doi.org/10.1016/j.chemer.2019.04.005>
- Serov, P., Portnov, A., Mienert, J., Semenov, P., and Ilatovskaya, P., Methane release from pingo-like features across the South Kara Sea shelf, An area of thawing offshore permafrost, *J. Geophys. Res. Earth Surf.*, 2015, vol. 120, pp. 1515–1529.  
<https://doi.org/10.1002/2015JF003467>
- Shearer, J.M., Macnab, R.F., Pelletier, B.R., and Smith, T.B., Submarine pingos in the Beaufort Sea, *Science*, 1971, vol. 174, no. 4011, pp. 816–818.
- Shpolyanskaya, N.A., *Plejstocen-golocenovaya istoriya razvitiya kriolitozony Rossijskoj Arktiki "glazami" podzemnyh l'dov* (Pleistocene–Holocene History of the Development of the Permafrost Zone of the Russian Arctic Through the “Eyes” of Permafrost), Moscow–Izhevsk: Inst. Komp. Issled., 2015.
- Tulapin, A.V., Rokos, S.I., and Dlugach, A.G., Seismic velocity modeling and dynamic analysis of the seismoacoustic images of PLF in Pechora Sea, in *Rel'ef i chetvertichnyye obrazovaniya Arktiki, Subarktiki i Severo-Zapada Rossii. Mater. Ezhegodn. konf. po rezul'tatam ekspeditsionnykh issledovaniy* (Relief and Quaternary Deposits of the Arctic, Subarctic, and North-West Russia. Proc. Annual Conf. on the Results of Expedition Research), St. Petersburg, 2021, Iss. 8, pp. 246–251.
- Viskunova, K.G., Kalenich, A.P., Markina, N.V., and Shkarubo, S.I., *Gosudarstvennaya geologicheskaya karta Rossiiskoi Federatsii masshtaba 1 : 1000000 (vtoroe pokolenie). Zapadno-Sibirskaya seriya. List R-38-40. Karta poleznykh iskopaemykh i prognoza neftegazonosnosti* (The 1 : 1000000 State Geological Map of the Russian Federation (2nd ed.). West Siberian Ser. Sheet R-38-40. Map of Mineral Resources and Oil and Gas Potential Forecast), St. Petersburg: Vseross. Nauchno-Issled. Geol. Inst., 2003.

**Publisher's Note.** Allerton Press remains neutral with regard to jurisdictional claims in published maps and institutional affiliations.  
AI tools may have been used in the translation or editing of this article.